

Global impacts of a Foreshock Bubble: Magnetosheath, magnetopause and ground-based observations

M. O. Archer^{a,1,*}, D. L. Turner^b, J. P. Eastwood^a, S. J. Schwartz^a, T. S. Horbury^a

^a*Space & Atmospheric Physics Group, The Blackett Laboratory, Imperial College London, Prince Consort Road, London, SW7 2AZ, UK.*

^b*Department of Earth, Planetary and Space Sciences, University of California, 603 Charles E. Young Drive, Los Angeles, California, CA 90095-1567, USA.*

Abstract

Using multipoint observations we show, for the first time, that Foreshock Bubbles (FBs) have a global impact on Earth's magnetosphere. We show that an FB, a transient kinetic phenomenon due to the interaction of backstreaming suprathermal ions with a discontinuity, modifies the total pressure upstream of the bow shock showing a decrease within the FB's core and sheath regions. Magnetosheath plasma is accelerated towards the the intersection of the FB's current sheet with the bow shock resulting in fast, sunward, flows as well as outward motion of the magnetopause. Ground-based magnetometers also show signatures of this magnetopause motion simultaneously across at least 7 hours of magnetic local time, corresponding to a distance of 21.5 R_E transverse to the Sun-Earth line along the magnetopause. These observed global impacts of the FB are in agreement with previous simulations and in stark contrast to the known localised, smaller scale effects of Hot Flow Anomalies (HFAs).

Keywords: Magnetosphere, Foreshock, Transient, Dynamics, Pressure

1. Introduction

Although Earth's bow shock primarily mediates the solar wind flow forming the magnetosheath, it is also an effective accelerator of energetic particles allowing a portion of those incident to travel back upstream along magnetic field lines forming Earth's foreshock (e.g. the review of Eastwood et al., 2005). The suprathermal backstreaming particles in this region, which is typically spatially extended upstream of the quasi-parallel shock (where the acute shock normal - magnetic field angle $\theta_{Bn} \lesssim 45^\circ$), cause kinetic instabilities within the incident solar wind plasma that can generate ultra-low frequency (ULF) waves (e.g. Hoppe et al., 1981) and in turn scatter particles. The foreshock is highly dynamic, due to variations in the interplanetary magnetic field (IMF) and solar wind conditions, and a number of kinetic phenomena resulting from the interaction of such changes with the quasi-parallel bow shock have been both simulated and observed. These foreshock transients, which include hot flow anomalies (Schwartz et al., 1985), foreshock cavities (Thomas and Brecht, 1988) and the recently discovered foreshock bubbles

*Corresponding author

Email address: m.archer10@imperial.ac.uk (M. O. Archer)

(Omidi et al., 2010), can have significant magnetospheric impacts such as perturbing the magnetopause (Sibeck et al., 1999; Turner et al., 2011) and generating magnetospheric ULF waves (Fairfield et al., 1990; Eastwood et al., 2011; Hartinger et al., 2013).

Foreshock Bubbles (FBs), first predicted by 2D kinetic hybrid simulations (Omidi et al., 2010, 2013; Karimabadi et al., 2014), are transient phenomena caused by the interaction of suprathermal backstreaming ions with a (rotational) discontinuity. Figure 1 shows an example schematic of how FBs are thought to form, following Turner et al. (2013). The motion of backstreaming ions, moving along the magnetic field and originating from the quasi-parallel bow shock, may be altered upon encountering a rotational discontinuity (RD). If the IMF cone angle θ_{Bx} (the angle between the IMF and the Sun-Earth line) is increased on the upstream side of this discontinuity, then the motional electric field $\mathbf{E} = -\mathbf{v}_{sw} \times \mathbf{B}$ will be greater and the backstreaming particles will experience increased $\mathbf{E} \times \mathbf{B}$ guiding centre drift \mathbf{v}_E equal to the component of the solar wind velocity perpendicular to the magnetic field (Greenstadt, 1976) i.e. with a component back towards the RD. In addition, the IMF change also results in the backstreaming ions' pitch angles increasing thereby converting some of the ions' motion parallel to the magnetic field into gyromotion. It can be shown (see Appendix A) in the deHoffmann-Teller rest frame of the RD (de Hoffmann and Teller, 1950), where the motional electric field is zero on both sides and thus particle energies are conserved, that the increase in particle pitch angle results in a concentration of suprathermal ion density upstream of the RD. Together with the increase in gyrospeed, the temperature and thermal pressure of the plasma increase upstream of the RD, thereby causing the thermal plasma to expand. Due to this expansion against the solar wind, a hot core region of depleted density and magnetic field with significant flow deflections forms immediately upstream of the RD followed by a compressed "sheath" region and possibly a shock. This whole structure, which convects with the RD whilst also growing, is what is known as a Foreshock Bubble.

The signatures of an FB in spacecraft observations, however, exhibit many similarities with Hot Flow Anomalies (HFAs): a transient phenomenon in the vicinity of the intersection of the bow shock with a (tangential) discontinuity due to kinetic shock processes (Schwartz et al., 1985, 1988; Thomsen et al., 1988; Paschmann et al., 1988). An HFA consists of a hot depleted core, usually on the side of the current sheet with quasi-parallel bow shock conditions (Omidi and Sibeck, 2007; Zhang et al., 2010; Wang et al., 2013b), sandwiched by compressions and sometimes shocks on both sides due to the lateral expansion of the plasma (Fuselier et al., 1987; Lucek et al., 2004). This structure tracks across the bow shock with a transit velocity given by (Schwartz et al., 2000)

$$\mathbf{v}_{trans} = \frac{\mathbf{v}_{sw} \cdot \mathbf{n}_{DD}}{\sin^2 \theta_{bs,DD}} (\mathbf{n}_{DD} - \cos \theta_{bs,DD} \mathbf{n}_{bs}) \quad (1)$$

where \mathbf{n}_{bs} and \mathbf{n}_{DD} are the normals to the bow shock and directional discontinuity (DD) respectively, $\theta_{bs,DD}$ is the angle between these and \mathbf{v}_{sw} is the solar wind velocity. Schwartz et al. (2000) summarised

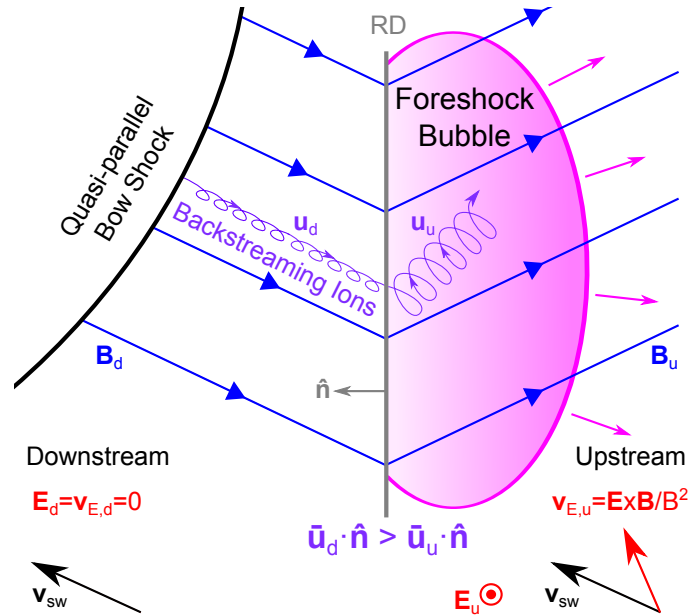


Figure 1: Example schematic of Foreshock Bubble formation. A rotational discontinuity (RD, grey) which increases the angle between the IMF (blue) and the Sun-Earth line on its upstream side results in an greater upstream motional electric field $\mathbf{E} = -\mathbf{v}_{sw} \times \mathbf{B}$ (red, out of the page). The motion of backstreaming ions in the foreshock on the downstream side of the RD is altered upstream, with a larger guiding centre drift \mathbf{v}_E (red arrow) back towards the RD as well as increased pitch angle due to the IMF change, resulting in an increase in the suprathermal density and temperature upstream of the RD. This increase in thermal pressure causes a local expansion, forming a Foreshock Bubble.

a set of conditions for the formation of HFAs, which required that the motional electric field points into the discontinuity on at least one side and that the transit speed of the discontinuity v_{trans} is much slower than the gyrospeed of ions reflected at the bow shock. Furthermore, they showed that HFAs preferentially occur if the discontinuity is tangential in nature (with no magnetic flux threading the current sheet), exhibits a small jump in magnetic field strength and quasi-perpendicular bow shock conditions are present on at least one side (with the upstream/trailing edge being favourable).

Turner et al. (2013) presented the first observational evidence of FBs upstream of Earth's bow shock, comparing and contrasting their signatures to HFAs. They developed a set of identification criteria to distinguish between the two phenomena:

1. HFA formation requires the discontinuity intersects with the bow shock; FB formation does not.
2. HFA cores form on the quasi-parallel side of the discontinuity or centred on the discontinuity if perpendicular/parallel on both sides (Omidi and Sibeck, 2007; Zhang et al., 2010; Wang et al., 2013b); FB cores should only form upstream of the discontinuity.
3. HFAs tend to be bounded on both sides by compression regions except theoretically when the ratio of incident suprathermal to solar wind ions $\gtrsim 65\%$ (Thomsen et al., 1988), though the strength of the compressions is often asymmetric with the upstream one typically being much larger (e.g. Paschmann et al., 1988); FBs observed from within the foreshock should be bounded by a compression region or shock on the upstream side only.
4. HFAs require the electric field point into the discontinuity on at least one side; FBs do not.

5. HFA boundaries can exhibit a range of orientations (Paschmann et al., 1988) though are often close to that of the discontinuity due to the lateral expansion of plasma; FB boundary normals observed from within the foreshock should be oriented predominantly sunwards.
6. HFAs move along the bow shock with the discontinuity intersection; FBs should convect with the solar wind.
7. HFAs have transverse sizes up to $\sim 4 R_E$ (Facskó et al., 2009) and their features are thought to diminish within $\sim 5 R_E$ of the bow shock (Wang et al., 2013a; Archer et al., 2014); FBs might have transverse scales comparable with the size of the quasi-parallel bow shock, $\sim 10 R_E$ or more (Omidi et al., 2010).

HFAs are known to have fairly localised impacts which track across the magnetosphere, including flow deflections in the magnetosheath, distortions of the magnetopause over $\sim 5 R_E$, and travelling convection vortices in the ionosphere (Sibeck et al., 1999; Eastwood et al., 2008; Jacobsen et al., 2009; Archer et al., 2014). In contrast, the impacts of FBs are predicted by simulations to be global in scale (Omidi et al., 2010): the arrival of the structure at the bow shock causes reversal of the magnetosheath flow back towards the FB core due to its reduced pressure compared to the magnetosheath plasma, in turn resulting in large scale outward motion of the magnetopause. Hartinger et al. (2013) presented observations of the magnetospheric response to an FB at a single spacecraft location, consisting of a rarefaction (due to the reduced dynamic pressure of the FB core) and then compression (due to the enhanced dynamic pressure of the FB sheath and shock) of the magnetospheric magnetic field and accompanied by Pc5 (2-7 mHz) ULF wave activity in the perpendicular components. However, the scale size of the magnetospheric impact of FBs has yet to be determined observationally. Since Pc5 ULF waves play a role in the mass, energy and momentum transport within the Earth’s magnetosphere e.g. accelerating electrons in auroral regions (Lotko et al., 1998) and the radiation belts (Claudepierre et al., 2013; Mann et al., 2013), it is important to understand the impacts of drivers of magnetospheric dynamics such as FBs. In this paper we present observationally, for the first time, the response of the magnetosheath and magnetopause to an FB, using multipoint spacecraft observations in conjunction with ground magnetometer measurements. We demonstrate the global nature of the transient’s impact, in agreement with the suggestion of previous simulations and in stark contrast to the known localised effects of HFAs.

2. Observations

2.1. Solar Wind & Foreshock

On 08 September 2008 at around 20:25 UT, two of the THEMIS (Angelopoulos, 2008) spacecraft were located in Earth’s foreshock at $14.3 R_E$ (THC) and $16.0 R_E$ (THB) upstream of the Earth. Figure 2b-d show high resolution (128 vectors s^{-1}) Fluxgate Magnetometer (FGM) data at THC in green. It is clear in the angles θ_{Bx} (the cone angle between the IMF and the GSE x-direction) and ϕ_B (the GSE

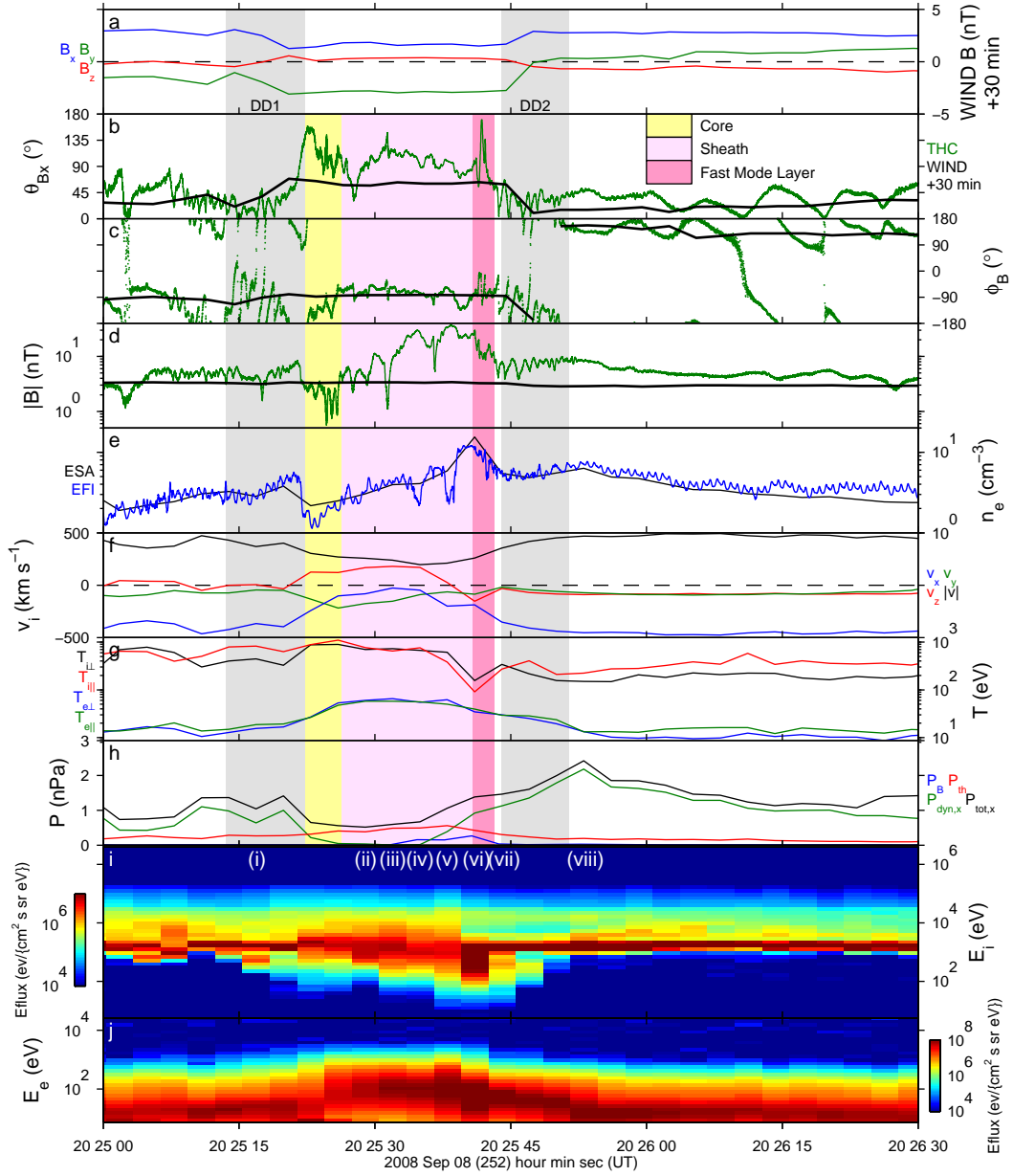


Figure 2: THC observations $\sim 1 R_E$ upstream of Earth's bow shock. From top to bottom: GSE magnetic field components in the pristine solar wind observed by WIND (xyz in blue, green, red) near L1 where data has been lagged by 30 min; comparisons between WIND (black) and THC (green) of the cone angle θ_{Bx} (between the magnetic field and the GSE x-direction), GSE clock angle ϕ_B , and magnetic field strength; electron density from ESA (black) and EFI (blue); GSE ion velocity components (xyz in blue, green, red) and magnitude (black); ion and electron temperatures parallel (red for ions, green for electrons) and perpendicular (black for ions, blue for electrons) to the magnetic field; magnetic (blue), thermal (red), anti-sunward dynamic (green) and total anti-sunward (black) pressures; ion and electron energy spectrograms where the colour scale represents the differential energy flux. Two directional discontinuities (DD1 & DD2) are highlighted in grey and core (yellow), sheath (light pink) and fast mode layer (pink) regions are also indicated.

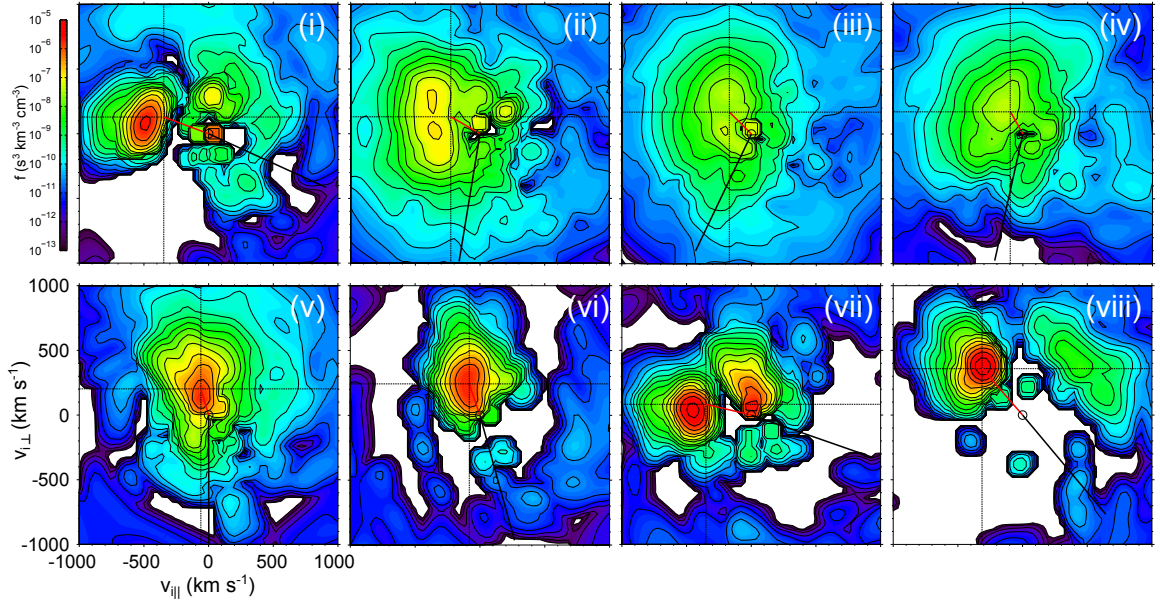


Figure 3: 2D cuts of ion distribution functions in the B-v plane at THC corresponding to the times indicated in Figure 2. The black circle denotes the origin in the spacecraft frame, the red line is the velocity moment and the black line shows the projection of the GSE x direction.

clock angle) that there were two directional discontinuities (DDs) which changed the IMF's orientation. We denote these as DD1 and DD2 and highlight them as the grey areas in Figure 2. The same directional discontinuities were also observed earlier by both ACE's Magnetic Field Experiment (Smith et al., 1998) (not shown) and WIND's Magnetic Field Investigation (Lepping et al., 1995) in the pristine solar wind near L1, with 30 min lagged data from the latter shown at 3 s resolution in black, revealing good agreement with the THC observations. Due to the proximity of the spacecraft to the subsolar bow shock, the IMF - shock normal angle θ_{Bn} magnetically connected to both THEMIS spacecraft was very similar to θ_{Bx} i.e. the bow shock was quasi-parallel before DD1, turning quasi-perpendicular between the two current sheets and subsequently returning to quasi-parallel conditions again. While the magnitude of the IMF as observed by WIND was relatively steady (panel d), THC observed strong variations in magnetic field strength following DD1: firstly decreasing sharply (yellow area), then increasing over ~ 12 s (light pink area), subsequently sharply dropping (dark pink area) before DD2 was observed and eventually returning to the ambient value after DD2.

Plasma data from ACE's Solar Wind Electron Proton Alpha Monitor (McComas et al., 1998) and WIND's Solar Wind Experiment (Ogilvie et al., 1995) revealed no strong variations (not shown due to their low time resolutions of 60 s and 97 s respectively). We present combined "burst" mode Electrostatic Analyzer (ESA) (McFadden et al., 2008a) and Solid State Telescope (SST) data (3 s cadence) at THC in Figure 2e-j, with corresponding 2D cuts of the ion distribution functions in the B-v plane shown in Figure 3. We also estimate the electron density from the $128 \text{ samples s}^{-1}$ spacecraft potential Electric Field Instrument (Bonnell et al., 2008) data using the method described by Chen et al. (2012) (shown in blue in panel e), which clearly reveal similar variations to $|\mathbf{B}|$. Large deflections of the ion velocity were observed

(panel f) during this event, predominantly because the x component almost went to zero, reducing the solar wind speed by about half. The electron temperatures parallel (green) and perpendicular (blue) to the magnetic field both increased inside the event (panel g). Figure 3i shows that before the event the ion distribution consisted of the solar wind beam along with intermediate backstreaming suprathermal ions characteristic of Earth’s foreshock (e.g. Fuselier, 1995). This backstreaming population results in the large parallel (red) temperature moment (over the entire distribution) in Figure 2g. In the depleted core region (yellow area in Figure 2) there was clearly an increase in the ion temperature, which also became more isotropic, and these hot, isotropic ion temperatures remained throughout the compressed “sheath” region (light pink), with the distributions (Figure 3ii-v) evolving to a single component plasma. Following the “sheath”, a correlated decrease in the density and magnetic field was observed (dark pink area in Figure 2) across which the velocity increased, returning to almost the solar wind speed. While such signatures are similar to that found exiting a shock transition into the unshocked upstream solar wind, the electron temperatures decreased smoothly rather than showing a sharp transition, and the ion temperature within this layer is actually lower than the upstream solar wind values. Due to these dissimilarities with shocks such as Earth’s bow shock, we shall refer to this transition simply as a fast mode layer (FML). Immediately upstream of the FML (Figure 3vii) the solar wind beam was observed once again along with a strong field aligned beam (comparable in phase space density to the solar wind), whereas following DD2 (Figure 3viii) an intermediate ion distribution was observed.

We calculate the combined isotropic ion and electron thermal pressure P_{th} (red), the magnetic pressure P_B (blue) and the anti-sunward dynamic pressure $P_{dyn,x}$ (green) as well as the sum of these, the total pressure $P_{tot,x}$ (black), with the results shown in Figure 2h. During the event the total pressure upstream of the bow shock was decreased from ~ 1.2 nPa to 0.5 nPa, principally because of the reduced dynamic pressure associated with the velocity deflections. A total pressure increase to ~ 2.4 nPa was also observed due to a slight density increase after DD2. While this might have been associated solely with DD2, it is possibly related to the transient event associated with DD1 since the FML (before DD2) did not return the density, magnetic field strength or electron temperatures to their ambient solar wind values.

We note that THB, less than $2 R_E$ further upstream than THC and separated transversely by $\sim 1 R_E$ in the y and $2.5 R_E$ in the z GSE directions, did not encounter strong variations between DD1 and DD2 when observed 52 s earlier (not shown). $|\mathbf{B}|$ decreased by ~ 2 nT, the density dropped by $\sim 1.6 \text{ cm}^{-3}$, no compressions were observed, the velocity was deflected by only $\sim 50 \text{ km s}^{-1}$ and ion temperature increases were $\sim 100 \text{ eV}$ (though in “reduced” mode as used here, ESA does not fully resolve the solar wind beam (McFadden et al., 2008a)).

2.1.1. Analysis

Despite the proximity of THC to the bow shock ($\sim 1.3 R_E$ upstream using the Shue et al. (1998) magnetopause model and the Farris and Russell (1994) bow shock standoff relation), the observed event

cannot be explained as being due to a breathing motion of the bow shock passing over the spacecraft: the density did not increase as quickly as the magnetic field in the “sheath” region (e.g. Schwartz et al., 2011), the greatest temperatures were observed in the region of decreased density and magnetic field, and the velocity contained strong transverse deflections inconsistent with a subsolar bow shock/magnetosheath encounter. This event was therefore a foreshock transient (e.g. Fairfield et al., 1990) associated with DD1 and here we perform further analysis in order to aid its classification.

To estimate the orientation of DD1 we employ three spacecraft timing (Horbury et al., 2001) using ACE, WIND and THC. We choose this method rather than four spacecraft triangulation (e.g. Schwartz, 1998) since the two THEMIS spacecraft were much closer together than those at L1. This computed normal $\mathbf{n}_{DD1} = (0.54, 0.56, 0.63)$ in GSE coordinates, resulted in agreement with the observed time lag between THB and THC to within $\sim 5^\circ$ of this orientation. The fraction of magnetic flux threading the current sheet $\mathbf{B} \cdot \mathbf{n}_{DD1} / |\mathbf{B}| \sim 0.2$ and the negligible change in $|\mathbf{B}|$ observed in the pristine solar wind mean that DD1 was an ED (either a tangential or rotational discontinuity) according to the classification of Neugebauer et al. (1984). The vast majority of solar wind current sheets are in this category (e.g. Knetter et al., 2004).

To estimate the normal to the FML we borrow methods from fast-mode shocks, namely magnetic coplanarity, velocity coplanarity (valid for high Mach shocks) and the three mixed mode normals (Schwartz, 1998). The resulting normals from all these methods were in excellent agreement at $\mathbf{n}_{FML} = (0.87, -0.31, -0.31)$ in GSE. From this normal we estimated the speed of the layer using both the conservation of mass (Schwartz, 1998) and continuity of the tangential electric field (c.f. Smith and Burton, 1988). Both methods again were in agreement resulting in a normal speed in the spacecraft frame $v_{FML} = -100 \text{ km s}^{-1}$. We calculate (using the speed and orientation of the FML along with the solar wind speed) that the transient was rapidly expanding in the x direction at $\sim 400 \text{ km s}^{-1}$.

Given the calculated orientations and speeds of DD1 and the FML, it is possible to construct 3D schematics of this event. These are shown in Figure 4 at different times, assuming that the FML was approximately planar over the spacecraft separations and that its speed remained constant. The bottom left and right panels shows when THC (green) observed DD1 and the FML respectively. In the former, it is clear that THC was downstream of the FML at this time. The top left panel corresponds to when THB (red) observed DD1, revealing that the FML was just downstream of the spacecraft at this time, which may explain why THB did not observe similar variations to THC.

2.1.2. Classification

The transient could have been a Hot Flow Anomaly (e.g. Schwartz et al., 2000): DD1 may have been tangential, it intersected the bow shock and the motional electric field pointed towards it on the upstream side (Figure 4). However, the depleted core was located on the side of the discontinuity with quasi-perpendicular bow shock conditions, whereas HFA cores are displaced to the quasi-parallel side

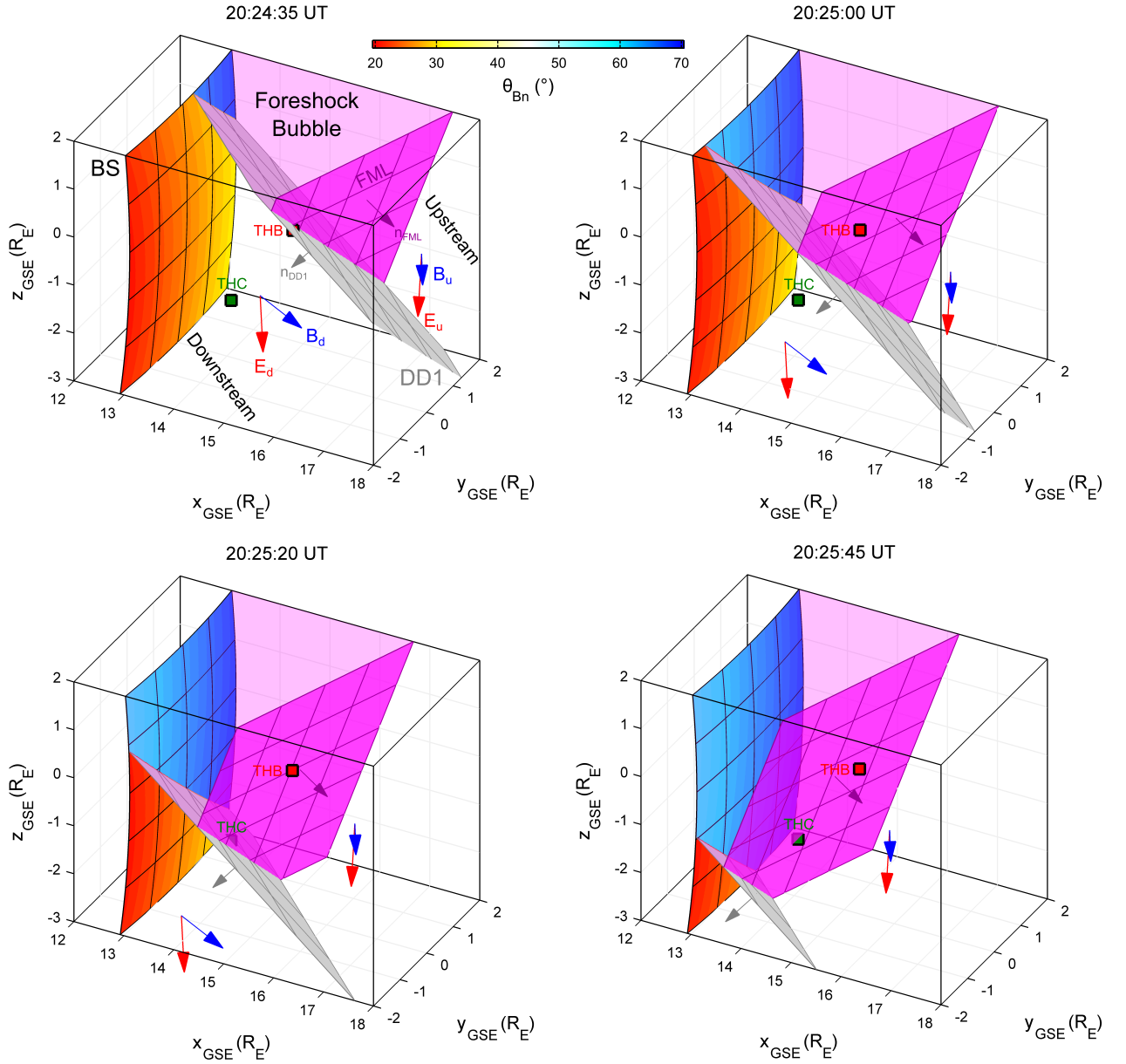


Figure 4: Schematics of the event in the solar wind/foreshock at different times. Spacecraft positions shown as the coloured squares. The current sheet DD1, with normal \mathbf{n}_{DD1} , and the fast mode layer (FML), with normal \mathbf{n}_{FML} , are shown in grey and magenta respectively. The Farris et al. (1991) model bow shock (BS) is coloured by the angle θ_{Bn} . The IMF (blue) and motional electric field (red) either side of DD1 are displayed as arrows.

(Omidi and Sibeck, 2007; Zhang et al., 2010; Wang et al., 2013b). If one assumes that the spacecraft observations were due to the transient moving across the bow shock, typical for HFAs (e.g. Facskó et al., 2009), then due to the orientations of \mathbf{v}_{trans} and \mathbf{n}_{FML} the observed core and “sheath” regions must have been being upstream of the FML. Such an arrangement is not consistent with the typical picture of HFAs from simulations (Lin, 2002) and observations (Lucek et al., 2004). Furthermore, DD1’s fast transit speed of $0.7\times$ the reflected ion gyrospeed (Schwartz et al., 2000), the lack of a significant compression on the downstream side of the transient given that the suprathermal ion density was 8% of the solar wind density (Thomsen et al., 1988), and the predominantly sunward orientation of the FML normal do not fit with the expected properties of an HFA at the subsolar bow shock.

Conversely, since DD1 may have been an RD and the IMF cone angle θ_{Bx} was increased on its upstream side, the event could have been a Foreshock Bubble (c.f. Figure 1). The location of the depleted core and the compression on the upstream side of DD1 are consistent with this, as is the sunward orientation of the FML (Turner et al., 2013). The transient therefore satisfied all the FB identification criteria of Turner et al. (2013) apart from the transverse size criterion, which we are unable to test due to no additional spacecraft observations of the transient. Henceforth we identify this event as a Foreshock Bubble.

2.2. Magnetosheath & Magnetopause

During this interval, another two of the THEMIS spacecraft (THD & THE) were located in the magnetosheath $\sim 1 R_E$ sunward of the Shue et al. (1998) model magnetopause, with THE slightly further away from the Earth by $\sim 0.2 R_E$, and separated by $\sim 1 R_E$ chiefly in the GSE y direction. Figure 5 shows combined “reduced” mode ESA and SST data (3 s resolution) as well as 4 vectors s^{-1} FGM data from the two spacecraft. In the latter we identify the transmitted discontinuities DD1 and DD2 (highlighted again by grey areas) by comparing the GSE y and z components with the WIND observations (Figure 2a). While THE (left) observed both of these, only DD2 could be clearly identified at THD (right). THE observed DD1 ~ 35 s later than it was observed at THD upstream of the bow shock, in fair agreement with the expected 45 s lag from two spacecraft timing given the current sheet’s estimated orientation (making the reasonable assumption that the magnetosheath did not significantly alter this (c.f. Sibeck et al., 2003)). Approximately centred around the transmitted discontinuity, THE (left) observed an enhancement of the magnetosheath flow speed (top panel, shaded in blue) from ~ 47 $km s^{-1}$ to ~ 107 $km s^{-1}$ lasting about $1^{3/4}$ min. This enhanced flow also exhibited large deflections such that the usual anti-sunward magnetosheath was accelerated both sunwards and in the GSE -y direction. At around the same time, a flow enhancement was also observed at THD (right) with a similar magnitude. On the other hand, the direction of the flow was only marginally sunward and exhibited some acceleration in the +z direction as well as the main deflection towards -y as with THE.

Again we calculate the thermal, magnetic, antisunward dynamic (for only those intervals in which

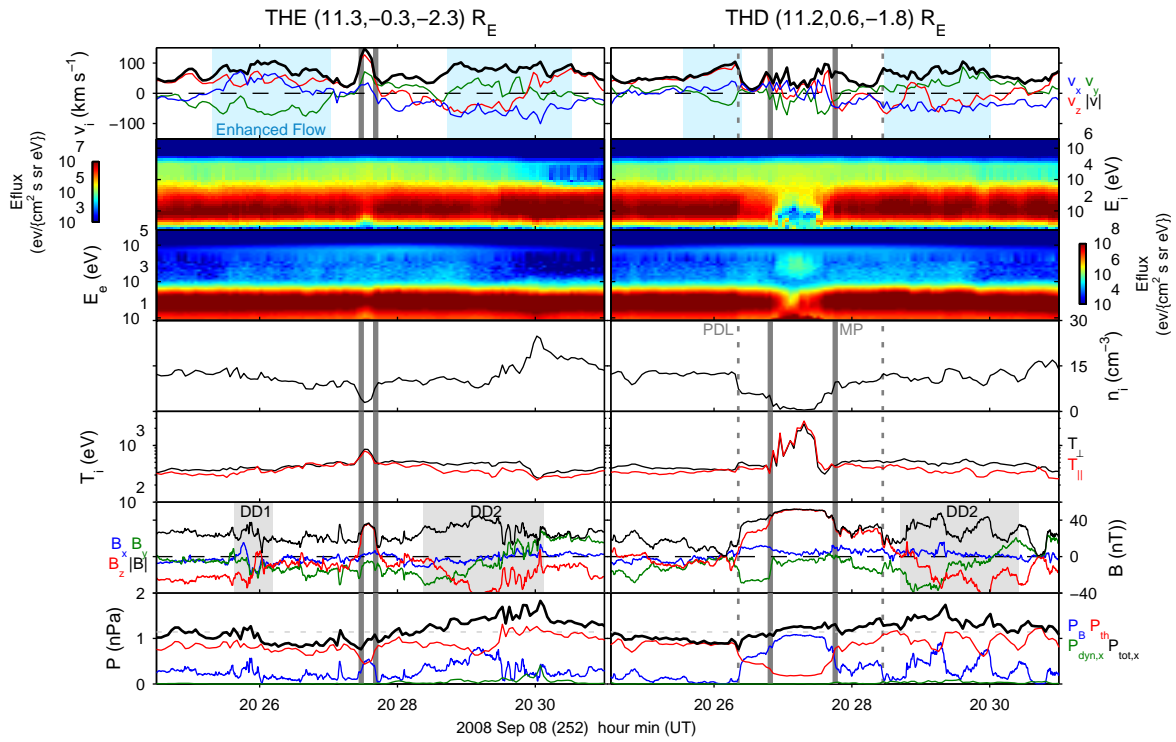


Figure 5: Magnetosheath observations from THE (left) and THD (right) with the spacecraft positions in GSE noted. From top to bottom: the ion velocity components in GSE (x, y, z in blue, green, red) and magnitude (black); ion energy spectrogram where the colour scale represents the differential energy flux; electron energy spectrogram; ion density; ion temperatures parallel (red) and perpendicular (black) to the magnetic field; magnetic field components in GSE (x, y, z in blue, green, red) and magnitude (black); and the magnetic (blue), thermal (red), anti-sunward dynamic (green) and total anti-sunward (black) pressures. The transmitted directional discontinuities DD1 and DD2, identified in Figure 2, are highlighted in grey. Blue shaded regions indicate enhanced magnetosheath flows, vertical solid grey lines correspond to magnetopause crossings and the vertical dotted line shows the edge of the plasma depletion layer.

the flow was antisunward) and total pressures in the magnetosheath as shown in the bottom panels of Figure 5. These reveal a total pressure decrease in the magnetosheath of ~ 0.3 nPa at 20:26, around the time of the enhanced flows. Whereas at THD (right) the pressure decrease is fairly gradual, at THE (left) this drop is sharp and follows the observation of the transmitted discontinuity DD1. This suggests that it was in response to the reduced total pressure associated with the FB that formed on the upstream side of this current sheet (Figure 2h).

Following the enhanced flow and pressure decrease, the magnetopause moved outwards causing THD (right) to enter into the plasma depletion layer (vertical dotted line) (Zwan and Wolf, 1976) between 20:26:20-20:26:50 UT, followed by the magnetopause passing over the spacecraft (solid vertical line). The spacecraft had a brief excursion in the magnetosphere before encountering the boundary again and returning to the magnetosheath at around 20:27:45 UT. In contrast, THE (slightly further from the model boundary) only partially encountered the magnetopause and did not fully cross the boundary into the magnetosphere.

We applied minimum variance analysis (MVA) (Sonnerup and Scheible, 1998) to spin-resolution FGM data to determine normals for the observed magnetopause crossings, testing the quality of the analysis via the intermediate-to-minimum eigenvalue ratio test ($\lambda_{int}/\lambda_{min} \gtrsim 10$ implying a reliable normal) as well as the sensitivity of the resulting normal to different time intervals centred on the boundary. Reliable normals could only be obtained for the THD crossings, since MVA was poorly conditioned at THE with $\lambda_{int}/\lambda_{min} \sim 2$. For the inbound case the obtained normal was deflected 18° from the Shue et al. (1998) model boundary, predominantly in the GSE +y direction, whereas for the outbound crossing the difference was only 6° i.e. consistent with being zero within errors (Sonnerup, 1971; Khrabrov and Sonnerup, 1998). These normals therefore suggest global/large scale motion of the magnetopause.

We estimate the normal speed of the boundary using the two spacecraft timing method (e.g. Schwartz, 1998). We apply this only to the inbound crossings, resulting in a speed of only ~ 20 km s $^{-1}$. While this method can be unreliable when the spacecraft separation is predominantly perpendicular to the boundary normal, as is the case here, the calculated speed is similar to the observed plasma velocity ahead of the boundary. By the time the magnetopause was observed by the spacecraft we deduce (both from the observed magnetosheath flow and the timing) that it had substantially decelerated. The boundary had moved outwards by $\sim 1 R_E$ from its nominal location, while a simple pressure balance calculation using the total pressure within the FB observed by THC (Figure 2h) results in an expected $1.6 R_E$ outward motion.

Figure 6 shows schematics of the magnetosheath and magnetopause response to the FB at different times in the GSE $z=-2 R_E$ plane. We indicate the observed magnetopause (black solid line) using the calculated normals (light blue arrows) at THD, the estimated magnetopause speed and the relative timings of the crossings at both spacecraft. It can be seen in the top right and bottom left panels that as

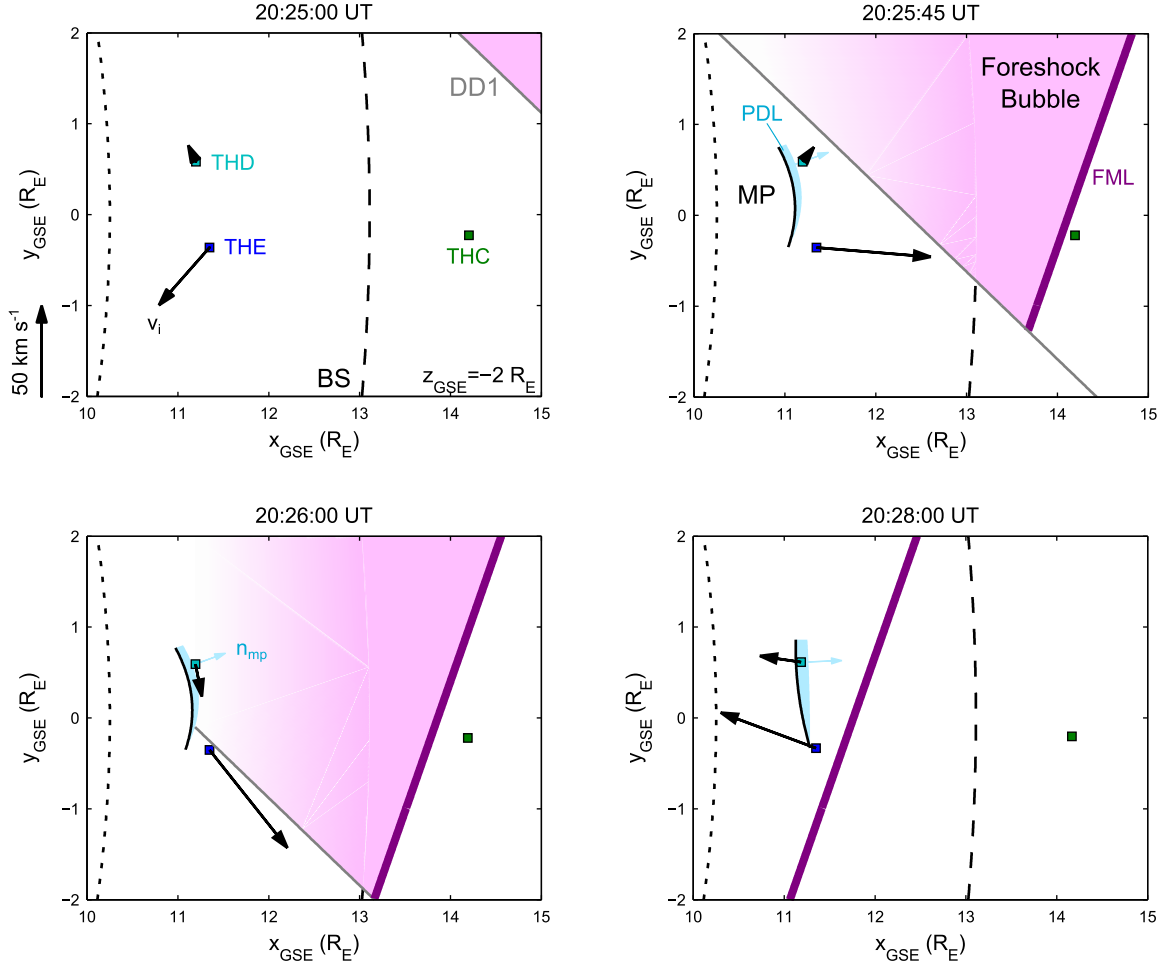


Figure 6: Schematics of the magnetosheath/magnetopause response in the GSE $z=-2 R_E$ plane at different times. Projections of the spacecraft positions are shown as the coloured squares. The Farris et al. (1991) bow shock and the Shue et al. (1998) magnetopause models are displayed as the dashed and dotted lines respectively, whereas the observed magnetopause (with normal \mathbf{n}_{mp}) is indicated by the solid black line along with the plasma depletion layer (light blue). The discontinuity DD1 (grey) and fast mode layer (magenta) are also shown. The observed ion velocities are given by the black arrows.

DD1 tracked across the bow shock in the vicinity of THD and THE, the magnetosheath flow (particularly at THE) was accelerated towards the location of the intersection of the current sheet with the shock.

Following the outbound crossing of the magnetopause at around 20:28:30-20:30:00 UT, both THD and THE again observed enhanced magnetosheath flows of similar magnitude and duration to those at 20:26 in the vicinity of DD1. The directions of these flows, however, was different being predominantly directed anti-sunwards. The enhanced flows coincided with the observations of DD2 at the spacecraft and the total pressure in the magnetosheath exhibited an enhancement of ~ 0.7 nPa. The timing of this pressure enhancement at the two magnetosheath spacecraft was consistent with the arrival of the FML at the spacecraft, again assuming unchanged orientation and speed (c.f. Sibeck et al., 2003), as shown in the bottom right panel of Figure 6. Thus the rapid expansion of the FB as it convected to the bow shock means that the ~ 45 s duration observations at THC upstream of the bow shock, resulted in the observed ~ 5 min duration impacts in the magnetosheath.

2.3. Ground-magnetometer

In addition to the spacecraft observations, we use ground magnetometer (GMAG) data across North America taken from the THEMIS, GIMA, CARISMA and CANMON networks in order to assess the scale of the magnetospheric impact of the FB. Figure 7 displays the H-component (horizontal component towards mean magnetic north) from all available GMAG stations at magnetic latitudes $65^\circ < \Lambda < 70^\circ$, ordered by magnetic local time (MLT). The one hour linear trend has been removed from each of these to highlight the variations. The data reveals a decrease followed by an increase at all stations, consistent with an outward followed by inward motion of the magnetopause. We estimate that the Alfvén travel time from the subsolar magnetopause to the FSMI GMAG (near noon MLT) was ~ 2 min using the T96 magnetic field model (Tsyganenko, 1995; Tsyganenko and Stern, 1996), in excellent agreement with the time delay between the spacecraft observations of the boundary and the extremum of the negative deflection observed on the ground.

The magnetic deflections were first observed and were strongest at GILL at around 14:00 MLT. This corresponds to a bow shock $\theta_{Bn} \sim 40^\circ$ (see Figure 4) i.e. approximately near the edge of the ion foreshock (Le and Russell, 1992). We associate this with the arrival of the FB at the bow shock/magnetopause. All the other stations observed deflections in quick succession. We plot the location of the intersection of DD1 with the Shue et al. (1998) magnetopause model as a function of time as the grey dashed line in Figure 7. This shows good agreement with the onset of the negative deflections at the GMAG stations at the subsolar and morning sectors. We also highlight the propagation of this magnetic impulse event through the circles in Figure 7, which indicate minima (blue) and maxima (red) from 2 min smoothed time series. Again these show that both the outward and inward disturbances of the magnetopause originated around 14:00 MLT and they subsequently propagated down both magnetopause flanks. While the timings in the morning sector are similar to that of the current sheet's transit across the dayside magnetopause, the later observation in the afternoon sector at KUUI cannot be explained in this way. This could either be due to the initial arrival of the FB at around 14:00 MLT launching a rarefaction wave down this flank similar to the magnetospheric response to the arrival of solar wind pressure pulses (Sibeck, 1990) or perhaps due to the spatial structure of the FB (see e.g Figure 1 or Omidi et al. (2010)).

By comparing the magnetic deflections observed by all stations at a given time, it is possible to estimate the instantaneous scale size of the magnetopause disturbance. For instance at around 20:30 UT B_H was reduced at all GMAG stations i.e. there was a large scale outward disturbance of the magnetopause from its nominal position spanning at least 7 hours of magnetic local time. Similarly at around 20:38 UT B_H was enhanced at all stations i.e. a large scale inward disturbance of the boundary. Using the Shue et al. (1998) model magnetopause, we find that these correspond to magnetopause disturbances spanning at least $21.5 R_E$ transverse to the Sun-Earth line.

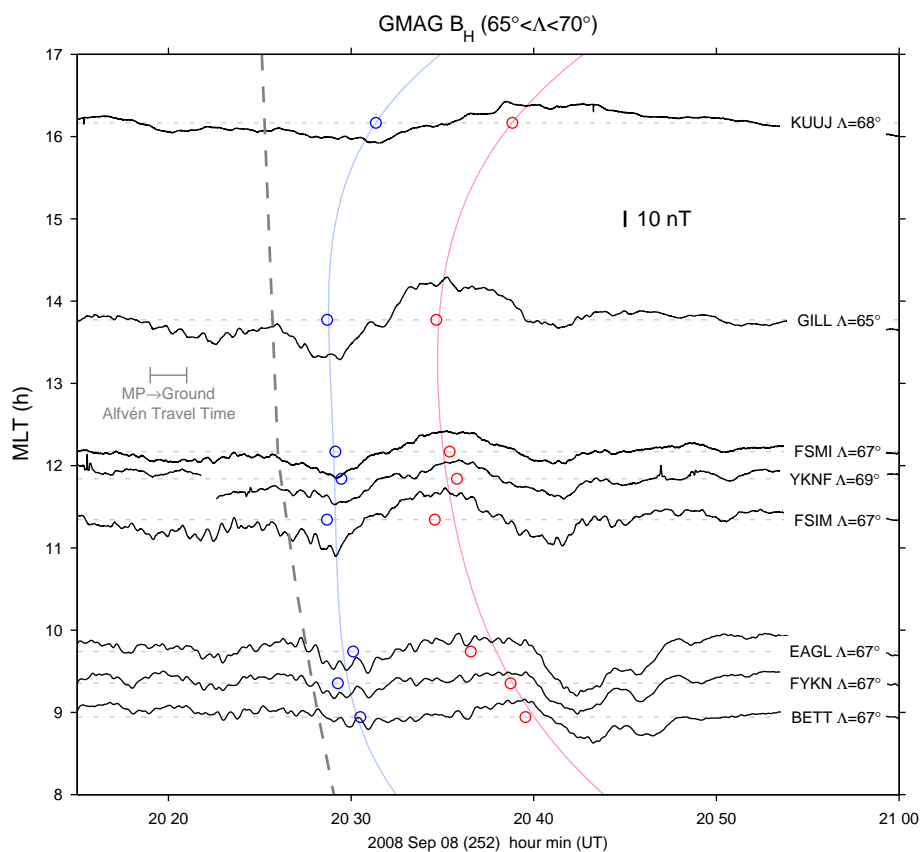


Figure 7: Stacked plots of the H-component of the magnetic field from ground-magnetometer stations ordered by the average magnetic local time (MLT), where the 1 hour linear trend has been removed. Station names and geomagnetic latitudes are noted. The minima (blue) and maxima (red) of the magnetic impulse event (from 2 min smoothed data) at each station are indicated by circles. The grey dashed line shows the intersection of DD1 with the Shue et al. (1998) model magnetopause in the GSE $z=-2 R_E$ plane and the Alfvén travel time from the subsolar magnetopause to the ground is also indicated.

3. Discussion

We have presented observations of a foreshock transient upstream of Earth’s bow shock along with simultaneous observations in the magnetosheath and on the ground showing its magnetospheric impacts. We concluded that the transient was unlikely to be an HFA, but that the observations were in agreement with the understood properties of FBs. Here we piece together all the observations, comparing the responses to those previously simulated (Omidi et al., 2010) as well as contrasting them with the known effects of HFAs (e.g. Sibeck et al., 1999).

Omidi et al. (2010) predicted that on arrival of an FB at the bow shock, the reduced total pressure of the FB core should cause a reversal of the magnetosheath flow back towards this low pressure region i.e. sunwards. Archer et al. (2014) observationally showed that the reduced total pressure upstream of the bow shock due to a foreshock transient (most likely an HFA) resulted in strong (thermal + magnetic) pressure gradients in the magnetosheath. They quantitatively demonstrated that these pressure gradients directly accelerated the magnetosheath plasma, causing fast sunward flows followed by outward magnetopause motion. Here we have shown that magnetosheath plasma was accelerated towards the intersection of the discontinuity with the bow shock, which quickly tracked across the bow shock. This point at the shock separates the original magnetosheath plasma (downstream) and the foreshock bubble plasma (upstream). Since the FB reduced the total pressure upstream of the bow shock, a pressure gradient must have existed. It is expected that this pressure gradient would accelerate magnetosheath plasma towards the intersection point, as observed. Whilst we cannot measure this pressure gradient due to a lack of spacecraft, we interpret the acceleration of the magnetosheath plasma towards this point as being directly driven by pressure forces (Archer et al., 2014) due to the arrival of the FB.

The large scale outward motion of the magnetopause reported here due to the FB’s reduced total pressure was also predicted in the Omidi et al. (2010) simulations. This is in stark contrast to the known effects of HFAs on the magnetopause. HFAs have dimensions across the bow shock of up to $\sim 4 R_E$ (Facsó et al., 2009), which result in similarly sized outward bulging of the boundary that moves with the HFA’s slow transit across the shock (Sibeck et al., 1999; Archer et al., 2014). Observational studies have identified these distortions from the determined boundary normals, revealing large deflections ($\geq 30^\circ$) from those expected by magnetopause models. In contrast, here the estimated boundary normals were close to the model ones, with at least the outbound crossing consistent with them being equal. Furthermore, the ascertained orientation of the inbound normal was inconsistent with that expected from a localised bulge of the magnetopause moving with the intersection of DD1 with the bow shock. The leading edge of such a bulge should be deflected from the model in the -y and -z GSE directions (e.g. Archer et al., 2014) given the orientation of DD1 (see Figure 6), however the observed (small) deflection was in the +y direction. Depending on the spacecraft location, normals aligned with the model boundary could be observed near the peak of the bulge due to an HFA. However, the GMAG data shows further evidence

against such localised bulging, given the magnetic deflections instantaneously spanned the equivalent of $21.5 R_E$ across the magnetopause.

The propagation and evolution of the magnetic impulse events observed by the GMAGs was also unlike that known for HFAs. These have been shown to move in agreement with the motion of their respective current sheets across the bow shock (Eastwood et al., 2008; Jacobsen et al., 2009), growing in time. This would correspond to a dusk to dawn motion. The effects of the FB were first observed at an MLT in agreement with the edge of the foreshock. Theoretically this is where the FB would first arrive at the bow shock (see Figure 1). The magnetic impulse event subsequently propagated tailward in both the dawn and dusk sectors, with decreasing amplitude. While the propagation dawnwards is in agreement with DD1's transit across the magnetopause, the duskwards propagation may be due to the FB's transverse structure (c.f. Figure 1, Omidi et al. (2010, 2013) and Karimabadi et al. (2014)) or through waves launched in the magnetosphere at the arrival of the transient.

4. Conclusions

We have presented a case study of the impacts of a foreshock transient on the magnetopause. From spacecraft observations upstream of the bow shock, we showed that the transient was largely inconsistent with a Hot Flow Anomaly (HFA). Instead it did agree with the understood properties of Foreshock Bubbles (FBs). The FB modified the upstream pressure of the solar wind, reducing the total pressure in its core and sheath regions. Due to these pressure variations the FB impinged upon the magnetosphere resulting in acceleration of magnetosheath plasma towards the intersection of the current sheet with the bow shock and large scale outward magnetopause motion spanning simultaneously at least 7 hours of magnetic local time, equivalent to $21.5 R_E$ transverse to the Sun-Earth line at the magnetopause. Therefore, we have shown for the first time that FBs, unlike other transient foreshock phenomena such as HFAs (e.g. Sibeck et al., 1999) or foreshock cavities (e.g. Turner et al., 2011), have large scale/global impacts upon the magnetosphere, similar to those of solar wind pressure pulses (e.g. Sibeck, 1990). It is not clear, however, in this event to what degree the large scale disturbance of the magnetopause is an effect of the FB's transverse scale size, which are simulated to be comparable to the extent of the quasi-parallel shock (Omidi et al., 2010), or the fast transit of the current sheet across the bow shock. Multi-spacecraft studies of further FB events and their magnetospheric impacts may help in this regard.

Magnetospheric ULF waves in the Pc5 (2-7 mHz) range generated by sudden changes in the solar wind dynamic pressure have recently been shown to have effects upon radiation belt electrons through bounce and drift resonances (Claudepierre et al., 2013; Mann et al., 2013). Foreshock transients, including FBs, are also a known source of Pc5 waves (Harteringer et al., 2013). By utilising the constellation of spacecraft currently in the near-Earth space environment (including Cluster, THEMIS, GOES and Van Allen Probes) it is now possible to investigate the role that foreshock transients, such as FBs, play in

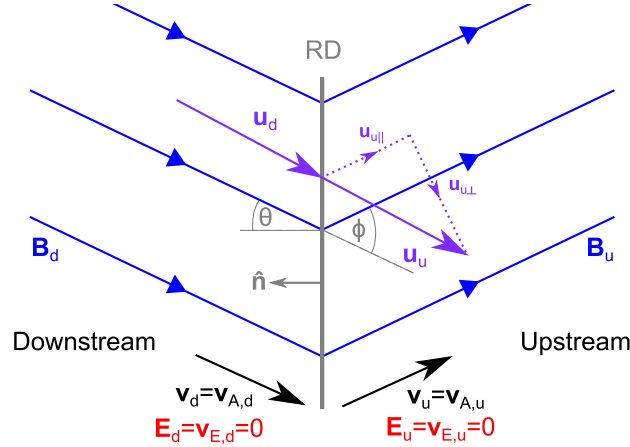


Figure A.8: deHoffman-Teller rest frame of a rotational discontinuity (RD, grey) in the same format as Figure 1.

terms of the radiation belts, which may form the subject of future work. While only a few examples of FBs have been reported in the literature, a statistical study into their occurrence and properties under different solar wind conditions could illuminate how often this recently discovered phenomenon occurs. Furthermore, additional simulations would also provide insight into their formation and large scale structure under different current sheet orientations.

Acknowledgements

M. O. Archer would like to thank C. H. K. Chen and H. Hietala for helpful discussions. This research at Imperial College London was funded by STFC grants ST/I505713/1, ST/K001051/1 and ST/G00725X/1. D. L. Turner is thankful for funding from NASA (THEMIS mission and grant NNX14AC16G). We acknowledge NASA contract NAS5-02099 and V. Angelopoulos for use of data from the THEMIS Mission, specifically C. W. Carlson and J. P. McFadden for use of ESA data; D. Larson and R. P. Lin for use of SST data; J. W. Bonnell and F. S. Mozer for use of EFI data; and K. H. Glassmeier, U. Auster and W. Baumjohann for the use of FGM data provided under the lead of the Technical University of Braunschweig and with financial support through the German Ministry for Economy and Technology and the German Center for Aviation and Space (DLR) under contract 50 OC 0302. We acknowledge A. Szabo and K. Ogilvie for WIND data; and N. Ness and D. McComas for ACE data. For GMAG data we thank the Geophysical Institute Magnetometer Array operated by the Geophysical Institute, University of Alaska; I.R. Mann, D.K. Milling and the rest of the CARISMA team, operated by the University of Alberta and funded by the Canadian Space Agency; The Canadian Magnetic Observatory Network (CANMON) maintained and operated by the Geological Survey of Canada; S. Mende, C. T. Russell and NSF for support through grant AGS-1004814.

Appendix A. Suprathermal density derivation

Here we derive the density of backstreaming suprathermal ions from the foreshock on the upstream side of a rotational discontinuity in its deHoffmann-Teller frame (de Hoffmann and Teller, 1950). In Figure A.8 we show an RD which rotates the tangential magnetic field by 180° for simplicity (the angle between the upstream and downstream fields $\phi = 2\theta$ in this case, where $0^\circ < \theta < 90^\circ$ is the angle between the magnetic field and the RD normal $\hat{\mathbf{n}}$), however we use the general case in our derivation whereby $0^\circ < \phi \leq 2\theta^\circ$. Since the electric field in this frame is zero on both sides, particle energies are conserved. Considering a single backstreaming ion with velocity \mathbf{u}_d on the downstream side, once it has crossed the RD the ion will instantaneously have a velocity on the upstream side \mathbf{u}_u given by (assuming the thickness of the RD is small relative to the upstream gyroradius):

$$\begin{aligned}\mathbf{u}_u &= \mathbf{u}_d \\ &= u_d \hat{\mathbf{B}}_d \\ &= u_d \cos \phi \hat{\mathbf{B}}_u + u_d \sin \phi \hat{\mathbf{u}}_{u\perp}\end{aligned}$$

i.e. the field-aligned guiding centre motion and a perpendicular component which is the particle's gyrovelocity since there are no perpendicular drifts in the deHoffmann-Teller frame. The incoming gyro-averaged particle flux (on the downstream side of the RD) is

$$\begin{aligned}F_{in} &= n_d \bar{\mathbf{u}}_d \cdot \hat{\mathbf{n}} \\ &= n_d u_d \cos \theta\end{aligned}$$

whereas the outgoing gyro-averaged flux (on the upstream side of the RD) is

$$\begin{aligned}F_{out} &= n_u \bar{\mathbf{u}}_u \cdot \hat{\mathbf{n}} \\ &= n_u u_d \cos \phi \hat{\mathbf{B}}_u \cdot \hat{\mathbf{n}} \\ &= n_u u_d \cos \phi \cos \theta\end{aligned}$$

where n is the number density of the particles under investigation here. Conservation of particles across the RD requires $F_{in} = F_{out}$ thus

$$\begin{aligned}n_d u_d \cos \theta &= n_u u_d \cos \phi \cos \theta \\ n_d &= n_u \cos \phi\end{aligned}$$

i.e. the density of the suprathermal particles upstream of the RD n_u is greater than that incident n_d .

Bibliography**References**

- Angelopoulos, V., 2008. The THEMIS mission. *Space Sci. Rev.* 141, 5–34.
- Archer, M. O., Turner, D. L., Eastwood, J. P., Horbury, T. S., Schwartz, S. J., 2014. The role of pressure gradients in driving sunward magnetosheath flows and magnetopause motion. submitted to *J. Geophys. Res.*
- Bonnell, J. W., Mozer, F. S., Delory, G. T., Hull, A. J., Ergun, R. E., Cully, C. M., Angelopoulos, V., Harvey, P. R., 2008. The electric field instrument (EFI) for THEMIS. *Space Sci. Rev.* 141, 303–341.
- Chen, C. H. K., Salem, C. S., Bonnell, J. W., Mozer, F. S., Bale, S. D., 2012. Density fluctuation spectrum of solar wind turbulence between ion and electron scales. *Phys. Rev. Lett.* 109, 035001.
- Claudepierre, S. G., Mann, I. R., Takahashi, K., Fennell, J. F., Hudson, M. K., Blake, J. B., Roeder, J. L., Clemmons, J. H., Spence, H. E., Reeves, G. D., Baker, D. N., Funsten, H. O., Friedel, R. H. W., Henderson, M. G., Kletzing, C. A., Kurth, W. S., MacDowall, R. J., Smith, C. W., Wygant, J. R., 2013. Van Allen Probes observation of localized drift resonance between poloidal mode ultra-low frequency waves and 60 keV electrons. *Geophys. Res. Lett.* 40, 4491–4497.
- de Hoffmann, F., Teller, E., 1950. Magneto-hydrodynamic shocks. *Phys. Rev. Lett.* 80, 692–703.
- Eastwood, J. P., Lucek, E. A., Mazelle, C., Meziane, K., Narita, Y., Pickett, J., Treumann, R. A., 2005. The foreshock. *Space Science Reviews* 118, 41–94.
- Eastwood, J. P., Schwartz, S. J., Horbury, T. S., Carr, C. M., Glassmeier, K.-H., Richter, I., Koenders, C., Plaschke, F., Wild, J. A., 2011. Transient Pc3 wave activity generated by a hot flow anomaly: Cluster, Rosetta, and ground-based observations. *J. Geophys. Res.* 116, A08224.
- Eastwood, J. P., Sibeck, D. G., Angelopoulos, V., Phan, T. D., Bale, S. D., McFadden, J. P., Cully, C. M., Mende, S. B., Larson, D., Frey, S., Carlson, C. W., Glassmeier, K.-H., Auster, H. U., Roux, A., Le Contel, O., 2008. THEMIS observations of a hot flow anomaly: solar wind, magnetosheath, and ground-based measurements. *Geophys. Res. Lett.* 35, L17S03.
- Facsó, G., Németh, Z., Erdős, G., Kis, A., Dandouras, I., 2009. A global study of hot flow anomalies using cluster multi-spacecraft measurements. *Ann. Geophys.* 27, 2057–2076.
- Fairfield, D. H., Baumjohann, W., Paschmann, G., Lühr, H., Sibeck, D. G., 1990. Upstream pressure variations associated with the bow shock and their effects on the magnetosphere. *J. Geophys. Res.* 95, 3773–3786.

- Farris, M. H., Petrinec, S. M., Russell, C. T., 1991. The thickness of the magnetosheath: Constraints on the polytropic index. *Geophys. Res. Lett.* 18, 1821–1824.
- Farris, M. H., Russell, C. T., 1994. Determining the standoff distance of the bow shock: Mach number dependence and use of models. *J. Geophys. Res.* 99, 17,681–17,689.
- Fuselier, S. A., 1995. Ion distributions in the earth's foreshock upstream from the bow shock. *Adv. Space Res.* 15, 43–52.
- Fuselier, S. A., Thomsen, M. F., Gosling, J. T., Bame, S. J., Russell, C. T., Mellott, M. M., 1987. Fast shocks at the edges of hot diamagnetic cavities upstream from the Earth's bow shock. *J. Geophys. Res.* 92, 3187–3194.
- Greenstadt, E. W., 1976. Energies of backstreaming protons in the foreshock. *Geophys. Res. Lett.* 3, 553–556.
- Hartinger, M. D., Turner, D. L., Plaschke, F., Angelopoulos, V., Singer, H., 2013. The role of transient ion foreshock phenomena in driving Pc5 ULF wave activity. *J. Geophys. Res.* 118, 299–312.
- Hoppe, M. M., Russell, C. T., Frank, L. A., Eastman, T. E., Greenstadt, E. W., 1981. Upstream hydro-magnetic waves and their association with backstreaming ion populations - ISEE 1 and 2 observations. *J. Geophys. Res.* 86, 4471–4492.
- Horbury, T. S., Burgess, D., Fränz, M., Owen, C. J., 2001. Three spacecraft observations of solar wind discontinuities. *Geophys. Res. Lett.* 28, 677–680.
- Jacobsen, K. S., Phan, T. D., Eastwood, J. P., Sibeck, D. G., Moen, J. I., Angelopoulos, V., McFadden, J. P., Engebretson, M. J., Provan, G., Larson, D., Fornaçon, K.-H., 2009. THEMIS observations of extreme magnetopause motion caused by a hot flow anomaly. *J. Geophys. Res.* 114, A08210.
- Karimabadi, H., Roytershteyn, V., Vu, H. X., Omelchenko, Y. A., Scudder, J., Daughton, W., Dimmock, A., Nykyri, K., Wan, M., Sibeck, D., Tatineni, M., Majumdar, A., Loring, B., Geveci, B., 2014. The link between shocks, turbulence, and magnetic reconnection in collisionless plasmas. *Phys. Plasmas* 21, 062308.
- Khrabrov, A. V., Sonnerup, B. U. Ö., 1998. Error estimates for minimum variance analysis. *J. Geophys. Res.* 103, 6641–6651.
- Knetter, T., Neubauer, F. M., Horbury, T., Balogh, A., 2004. Four-point discontinuity observations using Cluster magnetic field data: A statistical survey. *J. Geophys. Res.* 109, A06102.
- Le, G., Russell, C. T., 1992. A study of ULF wave morphology - I: ULF foreshock boundary. *Planet. Space Sci.* 40, 1203–1213.

- Lepping, R. P., Acuña, M. H., Burlaga, L. F., Farrell, W. M., Slavin, J. A., Schatten, K. H., Mariani, F., Ness, N. F., Neubauer, F. M., Whang, Y. C., Byrnes, J. B., Kennon, R. S., Panetta, P. V., Scheifele, J., Worley, E. M., 1995. The WIND magnetic field investigation. *Space Sci. Rev.* 71, 207–229.
- Lin, Y., 2002. Global hybrid simulation of hot flow anomalies near the bow shock and in the magnetosheath. *Planet. Space Sci.* 50, 577–591.
- Lotko, W., Streltsov, A. V., Carlson, C. W., 1998. Discrete auroral arc, electrostatic shock and suprathermal electrons powered by dispersive, anomalously resistive field line resonances. *Geophys. Res. Lett.* 25, 4449.
- Lucek, E. A., Horbury, T. S., Balogh, A., Dandouras, I., Rème, H., 2004. Cluster observations of hot flow anomalies. *J. Geophys. Res.* 109, A06207.
- Mann, I. R., Lee, E. A., Claudepierre, S. G., Fennell, J. F., Degeling, A., Rae, I. J., Baker, D. N., Reeves, G. D., Spence, H. E., Ozeke, L. G., Rankin, R., Milling, D. K., Kale, A., Friedel, R. H. W., Honary, F., 2013. Discovery of the action of a geophysical synchrotron in the Earth’s Van Allen radiation belts. *Nature Commun.* 4, 2795.
- McComas, D. J., Bame, S. J., Barker, P., Feldman, W. C., Phillips, J. L., Riley, P., Griffée, J. W., 1998. Solar wind electron proton alpha monitor (SWEPAM) for the Advanced Composition Explorer. *Space Sci. Rev.* 86, 563–612.
- McFadden, J. P., Carlson, C. W., Larson, D., Ludlam, M., Abiad, R., Elliott, B., Turin, P., Marckwordt, M., Angelopoulos, V., 2008a. The THEMIS ESA plasma instrument and in-flight calibration. *Space Sci. Rev.* 141, 277–302.
- Neugebauer, M., Clay, D. R., Goldstein, B. E., Tsurutani, B. T., Zwickl, R. D., 1984. A reexamination of rotational and tangential discontinuities in the solar wind. *J. Geophys. Res.* 89, 5395–5408.
- Ogilvie, K. W., Chornay, D. J., Fritzenreiter, R. J., Hunsaker, F., Keller, J., Lobell, J., Miller, G., Scudder, J. D., Sittler, E. C., J., Torbert, R. B., Bodet, D., Needell, G., Lazarus, A. J., Steinberg, J. T., Tappan, J. H., Mavretic, A., Gergin, E., 1995. SWE, a comprehensive plasma instrument for the WIND spacecraft. *Space Sci. Rev.* 71, 55–77.
- Omidi, N., Eastwood, J. P., Sibeck, D. G., 2010. Foreshock bubbles and their global magnetospheric impacts. *J. Geophys. Res.* 115, A06204.
- Omidi, N., Sibeck, D. G., 2007. Formation of hot flow anomalies and solitary shocks. *J. Geophys. Res.* 112, A01203.

- Omidi, N., Sibeck, D. G., Blanco-Cano, X., D., R.-C., Turner, D. L., Zhang, H., Kajdič, 2013. Dynamics of the foreshock compressional boundary and its connection to foreshock cavities. *J. Geophys. Res.* 118, 823–831.
- Paschmann, G., Haerendel, G., Scopke, N., Möbius, E., Lühr, H., Carlson, C. W., 1988. Three-dimensional plasma structures with anomalous flow directions near the earth's bow shock. *J. Geophys. Res.* 93 (A10), 11279–11294.
- Schwartz, S. J., 1998. Analysis Methods for Multi-Spacecraft Data. ISSI Scientific Reports SR-001. ESA Publications Division, Ch. Shock and discontinuity normals, Mach numbers, and related parameters, pp. 249–270.
- Schwartz, S. J., Chaloner, C. P., Christiansen, P. J., Coates, A. J., Hall, D. S., Johnstone, A. D., Gough, M. P., Norris, A. J., Rijnbeek, R. P., Southwood, D. J., Woolliscroft, L. J. C., 1985. An active current sheet in the solar wind. *Nature* 318, 269–271.
- Schwartz, S. J., Henley, E., J., M. J., 2011. Electron temperature gradient scale at collisionless shocks. *Phys. Rev. Lett.* 107, 215002.
- Schwartz, S. J., Kessel, R. L., Brown, C. C., Woolliscroft, L. J. C., Dunlop, M. W., Farrugia, C. J., Hall, D. S., 1988. Active current sheets near the earth's bow shock. *J. Geophys. Res.* 93 (A10), 11295–11310.
- Schwartz, S. J., Paschmann, G., Scopke, N., Bauer, T. M., Dunlop, M., Fazakerley, A. N., Thomsen, M. F., 2000. Conditions for the formation of hot flow anomalies at Earth's bow shock. *J. Geophys. Res.* 105, 12,639–12,650.
- Shue, J.-H., Song, P., Russell, C. T., Steinberg, J. T., Chao, J.-K., Zastenker, G., Vaisberg, O. L., Kokubun, S., Singer, H. J., Detman, T. R., Kawano, H., 1998. Magnetopause location under extreme solar wind conditions. *J. Geophys. Res.* 103, 17,691–17,700.
- Sibeck, D. G., 1990. A model for the transient magnetospheric response to sudden solar wind dynamic pressure variations. *J. Geophys. Res.* 95, 3755–3771.
- Sibeck, D. G., Borodkova, N. L., Schwartz, S. J., Owen, C. J., Kessel, R., Kokubun, S., Lepping, R. P., Lin, R., Liou, K., Luh, H., McEntire, R. W., Meng, C., Mukai, T., Nemecek, Z., Parks, G., Phan, T. D., Romanov, S. A., Safrankova, J., Sauvaud, J., Singer, H. J., Solov'ev, S. I., Szabo, A., Takahashi, K., Williams, D. J., Yumoto, K., Zastenker, G. N., 1999. Comprehensive study of the magnetospheric response to a hot flow anomaly. *J. Geophys. Res.* 104, 4577–4593.
- Sibeck, D. G., Trivedi, N. B., Zesta, E., Decker, R. B., Singer, H. J., Szabo, A., Tachihara, H., Watermann, J., 2003. Pressure-pulse interaction with the magnetosphere and ionosphere. *J. Geophys. Res.* 108, SMP 16–1 – SMP 16–12.

- Smith, C. W., L'Heureux, J., Ness, N. F., Acuña, M. H., Burlaga, L. F., Scheifele, J., 1998. The ACE magnetic fields experiment. *Space Sci. Rev.* 86, 613–632.
- Smith, E. J., Burton, M. E., 1988. Shock analysis: Three useful relations. *J. Geophys. Res.* 93, 2730–2734.
- Sonnerup, B. U. Ö., 1971. Magnetopause structure during the magnetic storm of september 24, 1961. *J. Geophys. Res.* 76, 6717–6735.
- Sonnerup, B. U. O., Scheible, M., 1998. Analysis Methods for Multi-Spacecraft Data. ESA Publications Division, Ch. Minimum and maximum variance analysis, pp. 185–220.
- Thomas, V. A., Brecht, S. H., 1988. Evolution of diamagnetic cavities in the solar wind. *J. Geophys. Res.* 93, 11341–11353.
- Thomsen, M. F., Gosling, J. T., Bame, S. J., Quest, K. B., Russell, C. T., Fuselier, S. A., 1988. On the origin of hot diamagnetic cavities near the earth's bow shock. *J. Geophys. Res.* 93 (A10), 11311–11325.
- Tsyganenko, N. A., 1995. Modeling the earth's magnetospheric magnetic field confined within a realistic magnetopause. *J. Geophys. Res.* 100, 5599–5612.
- Tsyganenko, N. A., Stern, D. P., 1996. Modeling the global magnetic field of the large-scale birkeland current systems. *J. Geophys. Res.* 101, 27187–27198.
- Turner, D. L., Eriksson, S., Phan, T. D., Angelopoulos, V., Tu, W., Liu, W., Teh, W. L., McFadden, J. P., Glassmeier, K. H., 2011. Multispacecraft observations of a foreshock-induced magnetopause disturbance exhibiting distinct plasma flows and an intense density compression. *J. Geophys. Res.* 116, A04230.
- Turner, D. L., Omid, N., Sibeck, D. G., Angelopoulos, V., 2013. First observations of foreshock bubbles upstream of Earth's bow shock: Characteristics and comparisons to HFAs. *J. Geophys. Res.* 118, 1552–1570.
- Wang, S., Zong, Q., Zhang, H., 2013a. Cluster observations of hot flow anomalies with large flow deflections: 1. velocity deflections. *J. Geophys. Res.* 118, 732–743.
- Wang, S., Zong, Q., Zhang, H., 2013b. Cluster observations of hot flow anomalies with large flow deflections: 2. bow shock geometry at HFA edges. *J. Geophys. Res.* 118, 418–433.
- Zhang, H., Sibeck, D. G., Zong, Q.-G., Gary, S. P., McFadden, J. P., Larson, D., Glassmeier, K.-H., Angelopoulos, V., 2010. Time History of Events and Macroscale Interactions during Substorms observations of a series of hot flow anomaly events. *J. Geophys. Res.* 115, A12235.
- Zwan, B. J., Wolf, R. A., 1976. Depletion of solar wind plasma near a planetary boundary. *J. Geophys. Res.* 81, 1636–1648.